American Mineralogist, Volume 99, pages 2138–2141, 2014

LETTER

Identification of hydrogen defects linked to boron substitution in synthetic forsterite and natural olivine†

JANNICK INGRIN[1,*], ISTVÁN KOVÁCS[2], ETIENNE DELOULE[3], ETIENNE BALAN[4], MARC BLANCHARD[4], SIMON C. KOHN[5] AND JOERG HERMANN[6]

[1]UMET, UMR CNRS 8207, Université de Lille1, Bât. C6, 59655 Villeneuve d'Ascq, France
[2]Geological and Geophysical Institute of Hungary, Budapest, Stefánia Street 14, H-1143, Hungary
[3]CRPG-CNRS, BP20, 54501 Vandœuvre les Nancy, France
[4]Institut de Minéralogie, de Physique des Matériaux, et de Cosmochimie, Sorbonne Universités, UPMC Univ Paris 06, CNRS UMR 7590, IRD UMR 206, MNHN, F-75005, Paris, France
[5]Department of Earth Sciences, University of Bristol, Queens Road, Bristol, BS8 1RJ, U.K.
[6]Research School of Earth Sciences, ANU, Canberra, ACT, 0200, Australia

ABSTRACT

Experimental and theoretical evidence for the coupled substitution of B and H in synthetic forsterite and a natural olivine is presented. The intensities of OH bands at 3704 cm^{-1} (//z), 3598 cm^{-1} (//x,y), and 3525 cm^{-1} (//x) in a heterogeneous B-doped synthetic forsterite crystal matches the zoning of B concentration measured by ion probe. The two anti-symmetric stretching vibrations of BO_3 groups occur at 1301 cm^{-1} (//x) and 1207 cm^{-1} (//z) for the ^{10}B and at 1256 and 1168 cm^{-1} for the ^{11}B isotope. A microscopic model of the mixed (B,H) defect that accounts for experimental observations is obtained from quantum mechanical calculations. The BO_3 group lies on the (O3-O1-O3) face of the vacant Si site and the H atom is bonded to the O2 atom at the remaining apex. The occurrence of the same OH bands associated with ν_3 BO_3 vibrations in a natural olivine sample from Pakistan confirms the occurrence of this defect in nature. The three diagnostic OH bands can be used as a signature of H associated with boron substitution in olivine and forsterite, leading to a quantitative analysis of their contribution to H-defects.

Keywords: Olivine, forsterite, FTIR, hydrogen, H-defects, boron, ^{10}B, ^{11}B, BO_3

INTRODUCTION

The coupled substitution of B and H for Si, formally written as $B(OH)Si_{-1}O_{-1}$, is not considered a major hydrogen incorporation mechanism in olivine because most natural samples contain too little B (less than a few wt. ppm B) (Kent and Rossman 2002). However, this mechanism could be dominant in samples with anomalously high B concentrations (Kent and Rossman 2002). It has once been proposed to explain a B-rich olivine from the Tayozhnoye Fe deposit in Russia (Grew et al. 1991; Sykes et al. 1994). Unfortunately, due to the presence of other types of OH defects in natural samples, significant uncertainty remains in the position of the OH bands associated with the $B(OH)Si_{-1}O_{-1}$ substitution and in the nature of the defect (Sykes et al. 1994). In addition, attempts to synthesize B-doped forsterite with associated H defects were not successful (Berry et al. 2007).

In this letter, we identify for the first time the coupled H and B substitution in a synthetic forsterite sample by experiment and theory. The corresponding defect generates characteristic infrared (IR) absorption bands, which compare well with those obtained from a quantum-mechanical modeling of mixed B and H defects in tetrahedral sites of forsterite. The IR analysis of a natural B-bearing olivine from the same origin as that studied by Gose et al. (2008, 2010) confirms the $B(OH)Si_{-1}O_{-1}$ substitution as a H-incorporation mechanism in nature.

* E-mail: Jannick.Ingrin@univ-lille1.fr

† Open access: Article available to all readers online.

SAMPLES AND METHODS

The forsterite crystal was synthesized by Lemaire et al. (2004) from hydrous melt at 2 GPa by cooling from 1400 to 1275 °C under medium-to-high silica activity. A single, unoriented, double-polished slice (~1.0 × 0.7 mm^2 and 240 μm thick) was used for IR measurements. A crystal from the same batch was studied by Ingrin et al. (2013). Two samples of B-bearing olivine from the Kaghan Valley (Pakistan) were used (Gose et al. 2010). One is the piece containing 72 wt. ppm H_2O described by Kovács et al. (2008). It is a parallelepiped of 1.882 × 1.936 × 1.962 mm^3 with faces perpendicular to the crystal axes, and was used for recording OH stretching bands. The other crystal was cut in two thin slices (380 and 285 μm thick) to study the polarization of the B-O stretching vibrations in the (x,y) and (x,z) planes, respectively. The OH IR signature of both samples is identical to the one reported by Gose et al. (2010). Previous TEM studies on the forsterite (Lemaire et al. 2004) and Pakistan olivine (Gose et al. 2010) have shown the absence of inclusions down to the sub-micrometer scale.

IR spectra were acquired with a Bruker Hyperion 3000 FTIR-microscope attached to a Bruker Vertex 70 spectrometer equipped with a liquid-N_2-cooled MCT detector in the laboratory of infrared and Raman spectrochemistry (LASIR, Université Lille 1). A Linkam FTIR600 heating-cooling stage with ZnSe windows was used for low-temperature conditions (see Ingrin et al. 2013 for more details). Spot sizes of 100 × 100 and 60 × 60 μm^2 were used for low-temperature and room-temperature measurements, respectively, and 256 scans were accumulated per spectrum. Polarized spectra were recorded with a wire grid polarizer on a KRS-5 substrate in the microscope.

The B content was determined with a Cameca IMS 1270 ion microprobe at CRPG. A 13 kV, 16 nA O^- primary beam was focused on a 25 μm diameter area, and the 10 kV positive secondary ions was measured at a mass resolution of 1500 with an energy offset of 60 V through an energy slit of 30 V. A single collector was used in ion-counting mode, and each analysis consisted of 25 successive cycles including the masses of 9.6 (for background), and those of ^{10}B, ^{11}B, and ^{30}Si (reference mass), with measurement times of 4, 8, 4, and 4 s, respectively (waiting time 1 s). The beam centering, and the mass and energy calibrations were checked before each measurement, after a 2 min presputtering. NBS 614, NBS 617, and UTR2 glasses

were used to determine the relative sensitivity factor of B/Si. The B/Si ratio for each spot was derived from the measured $^{11}B/^{30}Si$ ratio.

Theoretical calculations were performed within the density functional theory framework, using the approach and parameters of Balan et al. (2011, 2014). The ionic core of B was described by the norm-conserving pseudo-potential previously used in Ferlat et al. (2006).

Results and discussion

We discovered in a forsterite batch (run no. 6) synthesized by Lemaire et al. (2004) a heterogeneous single crystal displaying the whole range of OH bands observed among crystals from the same synthesis experiment (spectra 6a to 6e in Fig. 2 of Lemaire et al. 2004). Ion probe analyses show a strong B enrichment at the edge compared with the core of the crystal (160–230 vs. 2–4 wt. ppm, respectively). The presence of B is very probably linked to diffusion from the glass sleeve used in the high-pressure assembly. Significant differences are observed between the edge and core IR spectrum at room temperature (Fig. 1). The edge spectrum displays an additional strong OH band at 3598 cm^{-1} and weaker bands at 3525 and 3704 cm^{-1}. The broad band at 3216 cm^{-1} is also enhanced (Fig. 1a1), but its direct relationship with the presence of B is doubtful. The three bands at lower wavenumbers correspond to those observed at 3598, 3527, and 3220 cm^{-1} by Lemaire et al. (2004) with respective maximum intensities along y, x, and z axes. These OH bands have different thermal behaviors, leading to different shifts and narrowing at –194 °C (Fig. 1b1; Table 1). As previously reported, the strongest changes are observed for the 3598 cm^{-1} band (Ingrin et al. 2013). Similar OH bands have been observed in samples annealed in high-pressure assemblies surrounded by BN sleeves (Bollinger et al. 2014). Between 1050 and 1500 cm^{-1}, the edge spectrum displays four bands at 1301, 1256, 1207, 1167 cm^{-1}, and possibly two additional bands at 1156, 1132 cm^{-1} (Fig. 1a2, 1b2), which are not related to pure forsterite. The four intense bands are also observed in the samples studied by Lemaire et al. (2004); they are polarized along x (1301, 1256) and z (1207, 1167) (Fig. 2a). They occur in a frequency range where asymmetric ν_3 vibration modes of BO_3 groups are generally active (Weir and Schroeder 1964), which suggests the occurrence of BO_3 groups subparallel to the (x,z) plane. Considering the previously reported replacement of SiO_4 tetrahedra by BO_3 groups in synthetic anhydrous diopside and forsterite (Halenius et al. 2010a, 2010b), it is likely that BO_3 groups also occur in forsterite (the ν_3 bands in diopside are shifted to higher frequencies (>1300 cm^{-1}) due to the occurrence of B-O-Si linkages in the tetrahedral chains). The bands at 1167 and 1256 cm^{-1} in the forsterite spectra are similar to those at 1164 and 1257 cm^{-1} in the B-rich olivine from the Tayozhnoye deposit (Sykes et al. 1994). The bands at 1207 and 1301 cm^{-1} likely correspond to the isotopic shift of the bands at 1167 and 1256 cm^{-1}, respectively, due to ^{10}B (20.9 ± 0.1% from ion probe measurements). The ratios of the bands area support this interpretation (A_{1301}/A_{1256} = 22 ± 3%; A_{1207}/A_{1168} = 26 ± 10%). An estimate of the H content coupled to the B substitution at the crystal edge using the calibration coefficients of Kovács et al. (2010) (i.e., k = 0.57; [Si]) or Bell et al. (2003) gives ~150 ± 60 or 50 ± 20 wt. ppm H_2O, respectively; which requires the presence of either 180 ± 70 or 60 ± 25 wt. ppm B. Thus, the analysis of 160–250 wt. ppm of B at the crystal edge is consistent with a nearly stoichiometric coupled substitution of B and H.

To confirm the above interpretation, theoretical defect models were obtained by replacing a Si by a B atom and by setting one H atom on the O2 atom (*Pbnm* space group). Two stable defect configurations were obtained after energy minimization (Fig. 3; Table 2; CIF file in Electronic Annexes[1]). In the most stable B_H_1 configuration, the BO_3 group lies on the (O3-O1-O3) face of the tetrahedral site, inclined at 17° from the (x,y) plane in a simi-

Table 1. Characteristics of main OH bands linked to the presence of B

Mineral	ν (cm^{-1}) 25 °C (±4 cm^{-1})[a]	ν (cm^{-1}) −194 °C (±1 cm^{-1})[a]	Γ (cm^{-1}) 25 °C	Γ (cm^{-1}) −194 °C	Pleochroism
Forsterite	3704	3714	20	10	z
	3598	3617	22	4	y > x
	3525	3534	12	4	x
Olivine	3699	3709	28	19	z
	3598	3615	16–20	6	y > x
	3521	3530	28	22	x

Notes: Frequency (ν), FWHM (Γ), and pleochroism. [a] Spectral resolution used in the study.

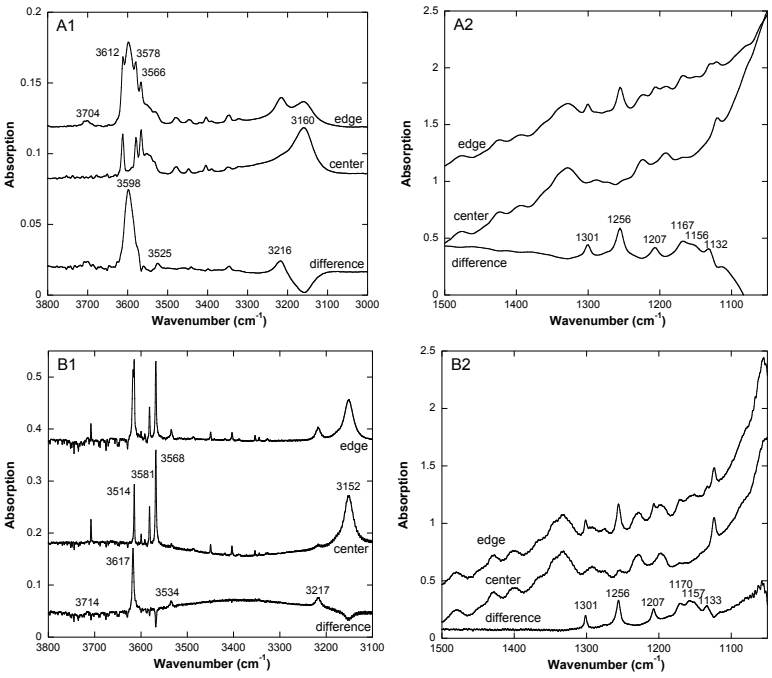

Figure 1. Unpolarized infrared spectra collected in the center and the edge of the forsterite slice and difference (edge – center) spectra, in the regions of O-H stretching bands (1) and B-O_x bands (2). (**a**) At room temperature. (**b**) At –194 °C.

[1] Deposit item AM-14-1017, CIF. Deposit items are stored on the MSA web site and available via the *American Mineralogist* Table of Contents. Find the article in the table of contents at GSW (ammin.geoscienceworld.org) or MSA (www.minsocam.org), and then click on the deposit link.

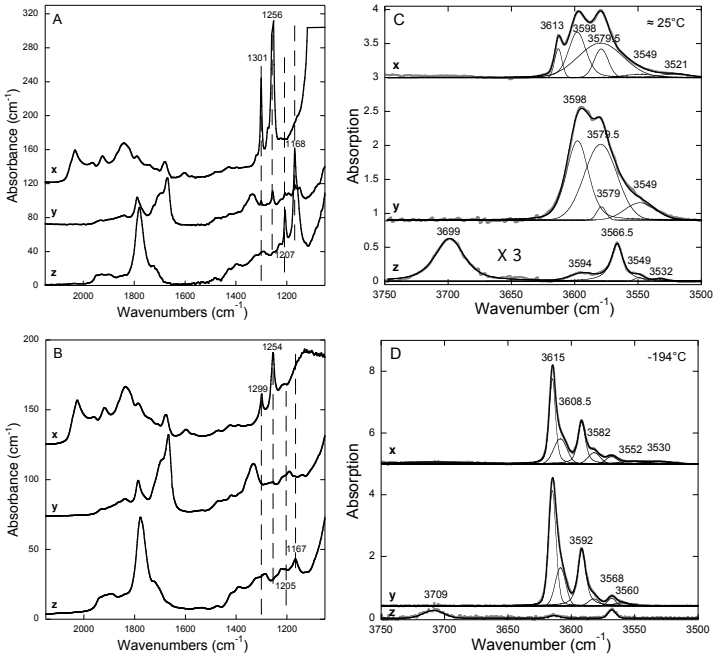

FIGURE 2. Room-temperature polarized IR spectra of the B-rich forsterite in the B-O_x regions (**a**) compared with polarized spectra of the olivine from Pakistan (**b**). Spectra in **a** are the same as in Figure 1 of Lemaire et al. (2004), with a larger spectral window. Deconvolution of OH bands in Pakistan olivine at room temperature (**c**) and –194 °C (**d**). Spectra are decomposed into Gaussian and Lorentzian individual bands using the PeakFit software. The spectrum polarized along z in **c** is multiplied by 3. The deconvolution of spectra polarized along x and y necessitates the presence of a low intensity band at 3579 cm^{-1} with a relatively narrow FWHM of 8–12 cm^{-1}. This is supported by the concomitant presence of the bands at 3613 cm^{-1} (x) and 3566.5 cm^{-1} (z); the three bands belonging to the $(4H)_{Si}$ defect (Balan et al. 2011; Ingrin et al. 2013).

lar way to CO_3 in the (F, CO_3) defect in apatite (Yi et al. 2013). The O2H group points out of the tetrahedral site. As expected from the theoretical approximation level, the theoretical B-O frequencies are underestimated by ~4% (e.g., Patton et al. 1997). However, the polarization and the splitting of the ν_3 B-O stretching modes and the corresponding isotopic shifts compare well with experiment (Table 2). The O2H stretching occurs at 3626 cm^{-1} and is dominantly polarized along y. It corresponds to the band measured at 3598 cm^{-1} (Fig. 3). The O2H geometry is similar to that of the O2H group in the $(4H)_{Si}$ defect model (Balan et al. 2011), explaining why its stretching frequency almost coincides with one from the $(4H)_{Si}$ defect at low temperature. Although not fully understood, the stronger temperature dependence of the B-related band probably stems from anharmonic coupling to a low-frequency vibration mode (Balan et al. 2014). This further confirms the importance of the local geometry of the defect in the control of anharmonic vibrational properties (Martin et al. 2006). The B_H_2 configuration is less stable by 26.5 kJ/mol, leading to a theoretical B_H_2/B_H_1 abundance ratio of ~12.7%. The O2-H group points to the O1 oxygen. It is dominantly polarized along x with stretching frequency of 3515 cm^{-1} (Fig. 3) and could correspond to the weaker band at 3525 cm^{-1}.

In the Pakistan olivine samples (Fig. 2b), the ν_3 B-O bands are observed at 1167 (z) and 1254 cm^{-1} (x) (1205 and 1299 cm^{-1} for ^{10}B) at room temperature. The OH contribution to the spectrum is complex and nine bands can be identified (Figs. 2c and 2d), among which three have frequencies, polarization, and temperature-induced shifts close to those ascribed to the mixed B and H defects in forsterite (Table 1). This confirms the original suspicions of Gose et al. (2010) and Mosenfelder et al. (2011) that this sample displays some OH bands associated with B-H substitution. These three bands at 3699, 3598, and 3521 cm^{-1} represent about 40% of the total OH band area in the Pakistan olivine spectra. They are superposed on the three bands ascribed to the $(4H)_{Si}$ defect (3613, 3579, and 3566.5 cm^{-1}; representing less than 10% of the OH band area), and to a broad band ascribed to interstitial OH groups (3549 cm^{-1} at

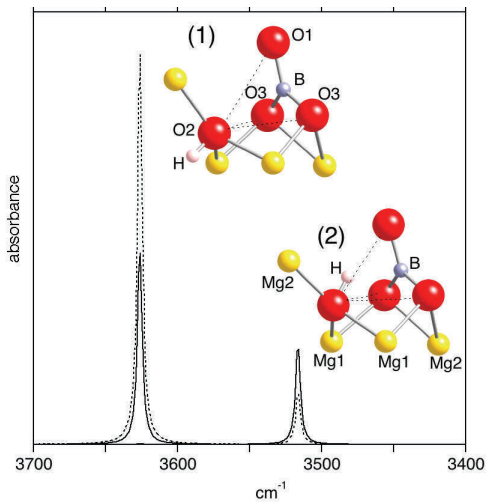

FIGURE 3. Theoretical structure of mixed (B,H) defects and theoretical IR absorption spectrum: (1) B_H_1 model (2) B_H_2 model. Solid line: x polarization; dotted line: y polarization. The spectrum of the B_H_2 model has been multiplied by 0.127 to account for its lower probability, assuming a Boltzmann statistic and a temperature of 1275 °C (i.e., the lower-end of the cooling ramp used in the synthesis experiments).

TABLE 2. Theoretical structure and vibrational properties of mixed B,H defects

Defect	dOH (Å)	OH stretching (cm^{-1})	K_{int} (OH stretching) ($Lmol^{-1}cm^{-2}$)	BO_3 angle (°)	ν_3 (x) ^{11}B (cm^{-1})	ν_3 (x) shift ^{10}B-^{11}B (cm^{-1})	ν_3 (z) ^{11}B (cm^{-1})	ν_3 (z) shift ^{10}B-^{11}B (cm^{-1})	ν_3 (x)–ν_3 (z) ^{11}B (cm^{-1})
B_H_1	0.980	3626 (3598) (A_y = 2 A_x)	15400	17.4	1207 (1256)	43.6 (45)	1119 (1168)	38.9 (39)	88 (88)
B_H_2	0.983	3516 (3525) (A_x = 1.9 A_y)	35900	14.6	1179	40.5	1134	38.5	45

Notes: dOH: O-H distance; A_x, A_y: OH stretching absorbance along x and y axes, respectively; K_{int}: integrated molar absorption coefficient, BO_3 angle with respect to the (100) axis, frequency, and polarization of ν_3 B-O bands for ^{11}B and ^{10}B isotopes. Relevant experimental values are indicated in parentheses.

room temperature; 3568 cm^{-1} at –194 °C) (Ingrin et al. 2013; Balan et al. 2014). Considering that the integral absorbance weakly depends on temperature, the broader contribution at 3579.5 cm^{-1} (FWHM ~30 to 40 cm^{-1}) at room temperature may correspond to the two bands at 3608.5 and 3592 cm^{-1} at –194 °C. There is no indication that these bands are linked to the presence of B. The significant proportion of B-associated OH bands in the Pakistan olivine brings into question the IR absorbance calibration for [Si] substitution proposed by Kovács et al. (2010). Their [Si] calibration factor (k = 0.57) more likely represents that of OH bands linked to B substitution. The "sensu strict" [Si] calibration factor may be closer to that of Bell et al. (2003) calibration or even lower (Withers et al. 2012).

Our results provide strong evidence for the coupled substitution of H and BO_3 for silica tetrahedra in synthetic forsterite and a natural olivine. The related defects can be quantitatively determined by three OH bands at ~3700, 3600, and 3520 cm^{-1} with specific polarizations. Note that a band not linked to B and mainly polarized along x, instead of y, is sometimes observed at ~3600 cm^{-1} in olivine (e.g, Withers et al. 2011). Although not fully understood, the pleochroic band at 3700 cm^{-1} is systematically observed in B-rich samples. As TEM studies ruled out the presence of serpentine or amphibole inclusions (which also lead to different spectral features; Miller et al. 1987; Matsyuk and Langer 2004), this band is likely related to B substitution and could be a fingerprint of OH and B association. Further confirmation of the presence of B can be gained from the ν_3 BO_3 vibrations at 1150–1350 cm^{-1}. We provide evidence for the isotopic splitting of the infrared ν_3 vibration bands of BO_3 groups, which has previously received insufficient attention in the study of B-rich/doped minerals. The present results confirm the usefulness of a detailed FTIR analysis to identify the complexity of H-defects in nominally anhydrous minerals and represent a significant step toward a complete identification of H-defects in mantle olivine and the understanding of their specific effects on the properties of peridotites. This Letter also highlights the importance of chemically composite defects at tetrahedral sites in the incorporation of volatile elements (H, B, F) in minerals (Crépisson et al. 2014). It confirms that the incorporation of planar molecular groups on the triangular face of tetrahedral sites is more common than originally thought (e.g., Halenius et al. 2010b; Yi et al. 2013).

Acknowledgments

This work was supported by the ANR grant (NT09-566853) provided to J. Ingrin and by the Bolyai Postdoctoral Fellowship Program and a postdoctoral grant (PD101683) of the Hungarian Scientific Research Found provided to I. Kovács. The PULI spectral database (puli.mfgi.hu) provided digital spectra. We thank Ian Swainson, Fabio Bellatreccia, and Henrik Skogby for their helpful suggestions to improve the manuscript.

References cited

Balan, E., Ingrin, J., Delattre, S., Kovács, I., and Blanchard, M. (2011) Theoretical infrared spectrum of OH-defects in forsterite. European Journal of Mineralogy, 23, 285–292.

Balan, E., Blanchard, M., Lazzeri, M., and Ingrin, J. (2014) Contribution of interstitial OH groups to the incorporation of water in forsterite. Physics and Chemistry of Minerals, 41, 105–114.

Bell, D.R., Rossman, G.R., Maldener, J., Endisch, D., and Rauch, F. (2003) Hydroxide in olivine: A quantitative determination of the absolute amount and calibration of the IR spectrum. Journal of Geophysical Research, 108, 2105–2113.

Berry, A.J., O'Neill, H.St.C., Hermann, J., and Scott, D.R. (2007) The infrared signature of water associated with trivalent cations in olivine. Earth and Planetary Science Letters, 261, 134–142.

Bollinger, C., Raterron, P., Cordier, P., and Merkel, S. (2014) Polycrystalline olivine rheology in dislocation creep: Revisiting experimental data to 8.1 GPa. Physics of the Earth and Planetary Interiors, 228, 211–219.

Crépisson, C., Blanchard, M., Bureau, H., Sanloup, C., Withers, A.C., Khodja, H., Surblé, S., Raepsaet, C., Béneut, K., Leroy, C., Giura, P., and Balan, E. (2014) Clumped fluoride-hydroxyl defects in forsterite: implications for the upper-mantle. Earth and Planetary Science Letters, 390, 287–295.

Ferlat, G., Cormier, L., Mauri, F., Balan, E., Charpentier, T., Anglada, E., and Calas, G. (2006) Ab initio calculations on borate systems. European Journal of Glass Science and Technology B, 4, 441–444.

Gose, J., Reichart, P., Dollinger, G., and Schmädicke, E. (2008) Water in natural olivine determined by proton-proton scattering analysis. American Mineralogist, 93, 1613–1619.

Gose, J., Schmädicke, E., Markowitz, M., and Beran, A. (2010) OH point defects in olivine from Pakistan. Mineralogy and Petrology, 99, 105–111.

Grew, E.S., Pertsev, N.N., Boronikhin, V.A., Borisovskiy, S.Y., Yates, M.G., and Marquez, N. (1991) Serendibite in the Tayozhnoye deposit of the Aldan Shield, eastern Siberia, U.S.S.R. American Mineralogist, 76, 1061–1080.

Halenius, U., Skogby, H., Eden, M., Nazzareni, S., Kristiansson, P., and Resmark, J. (2010a) Coordination of boron in nominally boron-free rock forming silicates: Evidence for incorporation of BO_3 groups in clinopyroxene. Geochimica et Cosmochimica Acta, 74, 5672–5679.

Halenius, U., Skogby, H., and Kristiansson, P. (2010b) Evidence for BO_3-groups in nominally boron-free minerals (NBFM) of mantle affinity. IMA 2010, Acta Mineralogical-Petrographica, Abstract series, 6, 484.

Ingrin, J., Liu, J., Depecker, C., Kohn, S.C., Balan, E., and Grant, K.J. (2013) Low-temperature evolution of OH bands in synthetic forsterite, implication for the nature of H-defects at high pressure. Physics and Chemistry of Minerals, 40, 499–510.

Kent, A.J.R., and Rossman, G.R. (2002) Hydrogen, lithium, and boron in mantle-derived olivine: The role of coupled substitutions. American Mineralogist, 87, 1432–1436.

Kovács, I., Hermann, J., O'Neill, H.St.C., Fitz Gerald, J. Sambridge, M., and Horváth, G. (2008) Quantitative absorbance spectroscopy with unpolarized light: Part II. Experimental evaluation and development of a protocol for quantitative analysis of mineral IR spectra. American Mineralogist, 93, 765–778.

Kovács, I., O'Neill, H.St.C., Hermann, J., and Hauri, E.H. (2010) Site-specific infrared O-H absorption coefficients for water substitution into olivine. American Mineralogist, 95, 292–299.

Lemaire, C., Kohn, S.C., and Brooker, R.A. (2004) The effect of silica activity on the incorporation mechanism of water in synthetic forsterite: a polarised infrared spectroscopic study. Contributions to Mineralogy and Petrology, 147, 48–57.

Martin, K.R., Blaney, P., Shi, G., Stavola, M., and Fowler, W.B. (2006) Temperature dependence of the vibrational spectrum of a Li-OH complex in ZnO: Infrared absorption experiments and theory. Physical Review B, 73, 232509.

Matsyuk, S.S., and Langer, K. (2004) Hydroxyl in olivines from mantle xenoliths in kimberlites of the Siberian platform. Contributions to Mineralogy and Petrology, 147, 413–437.

Miller, G.H., Rossman, G.R., and Harlow, G.E. (1987) The natural occurrence of hydroxide in olivine. Physics and Chemistry of Minerals, 14, 461–472.

Mosenfelder, J.L., Le Voyer, M., Rossman, G.R., Guan, Y., Bell, D.R., Asimov, P.D., and Eiler, J.M. (2011) Analysis of hydrogen in olivine by SIMS: Evaluation of standards and protocol. American Mineralogist, 96, 1725–1741.

Patton, D.C., Porezag, D.V., and Pederson, M.R. (1997) Simplified generalized-gradient approximation and anharmonicity: Benchmark calculations on molecules. Physical Review B, 55, 7454–7459.

Sykes, D., Rossman, G.R., Veblen, D.R., and Grew, E.S. (1994) Enhanced H and F incorporation in borian olivine. American Mineralogist, 79, 904–908.

Weir, C.E., and Schroeder, R.A. (1964) Infrared spectra of the crystalline inorganic borates. Journal of Research of the National Bureau of Standards, 68A, 465–487.

Withers, A.C., Hirschmann, M.M., and Tenner, T.J. (2011) The effect of Fe on olivine H_2O storage capacity: Consequences for H_2O in the martian mantle. American Mineralogist, 96, 1039–1053.

Withers, A.C., Bureau, H., Raepsaet, C., and Hirschmann, M.M. (2012) Calibration of infrared spectroscopy by elastic recoil detection analysis of H in synthetic olivine. Chemical Geology, 334, 92–98.

Yi, H., Balan, E., Gervais, C., Segalen, L., Fayon, F., Roche, D., Person, A., Morin, G., Guillaumet, M., Blanchard, M., Lazzeri, M., and Babonneau, F. (2013) A carbonate-fluoride defect model for carbonate-free fluorapatite. American Mineralogist, 98, 1066–1069.

Manuscript received May 12, 2014
Manuscript accepted June 8, 2014
Manuscript handled by Ian Swainson